Finite element simulation of the steel plates hot rolling process

Miguel A. Cavaliere, Marcela B. Goldschmit and Eduardo N. Dvorkin[*,†]

Center for Industrial Research, FUDETEC, Av. Córdoba 320, 1054, Buenos Aires, Argentina

SUMMARY

In this paper we discuss our finite element procedure for simulating the hot rolling of flat steel products. We couple an Eulerian rigid-viscoplastic model of the steel plates deformation to a Lagrangian elastic model of the rolls deformation. This latter model incorporates the bending deformation of the work rolls supported by the back-up rolls and the flattening of the contact areas (Hertz problem) via an enhanced beam model.

The finite element model is validated comparing its predictions with actual industrial measurements and then it is used to analyse different rolling set-ups. Copyright © 2001 John Wiley & Sons, Ltd.

KEY WORDS: metal forming; hot strip rolling; finite elements; thermal crown; roll bending; roll flattening

1. INTRODUCTION

In previous publications [1–6] we presented an Eulerian formulation for modelling metal forming processes which is based on the flow formulation (rigid-viscoplastic material models) [7] implemented via Thompson's pseudo-concentrations technique [8, 9]. When developing a 3D finite element model, for simulating the hot rolling of steel plates, it is necessary to include in this model the rolls deformation, because it plays a central role in determining the resulting *profile* and *flatness*[‡] of the rolled plates [10]. It can be safely assumed that the rolls (work and back-up rolls as per Figure 1) deform within the elastic range; hence, it is necessary to couple the Eulerian rigid-viscoplastic model of the rolled steel plates deformation to an elastic Lagrangian model of the rolls deformation.

*Correspondence to: Eduardo N. Dvorkin, Center for Industrial Research, FUDETEC, Av. Córdoba 320, 1054, Buenos Aires, Argentina
†E-mail: dvk@siderca.com
‡The concepts of plate profile and flatness will be discussed in Appendix A
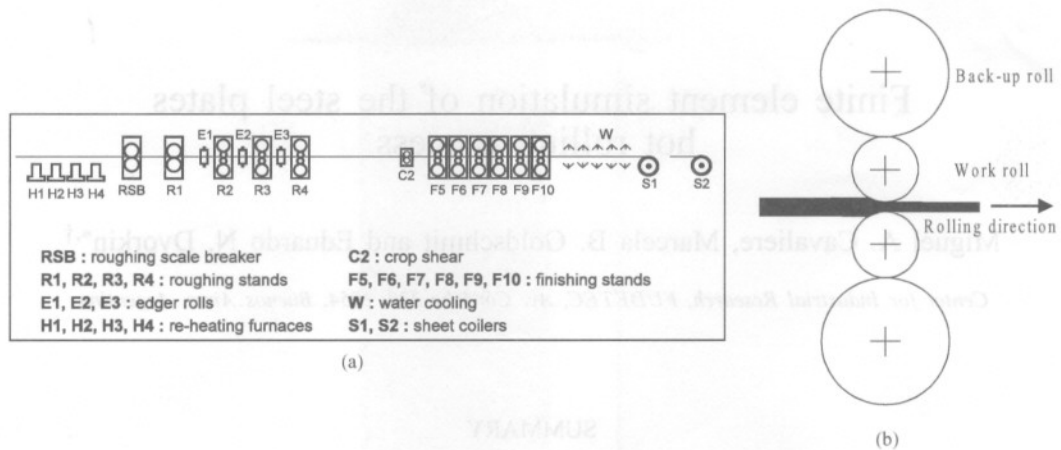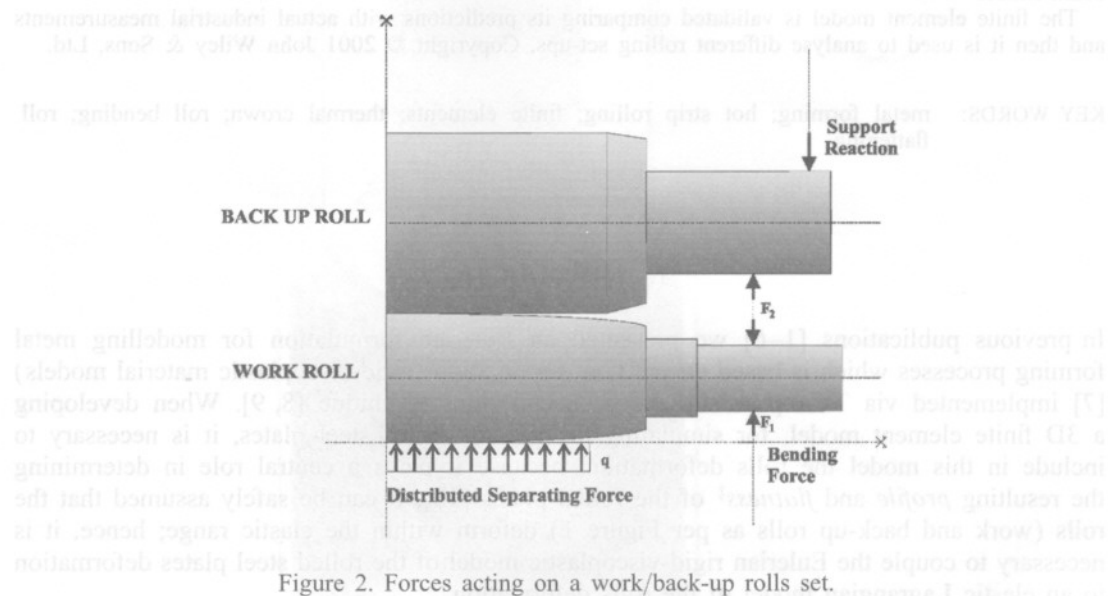
Figure 1. Typical hot rolling mill for steel plates: (a) diagram of a hot rolling mill for steel plates; (b) diagram of a 4-roll stand (R2 to F10 in the above diagram).

Figure 2. Forces acting on a work/back-up rolls set.

In the second section of this paper we summarize the relevant aspects of our Eulerian rigid-viscoplastic formulation and of its coupling to the elastic Lagrangian model that describes the rolls deformation under the loading indicated in Figure 2 (F_1 and F_2 are forces introduced by an hydraulic rolls bending system; this device is used to control the plates profile and flatness [10]).

When modelling the rolls deformation we assume a linear elastic material behaviour; however, we consider several geometrical non-linearities: contact between the work and back-up

rolls and flattening of the contact areas (Hertz problem). The simulation of these phenomena is achieved using an enhanced beam model rather than a more expensive 3D model of the rolls.

In the third section of this paper we present a detailed description of the non-linear enhanced beam model that we developed for simulating the rolls deformation.

With the coupled formulation implemented in our finite element code METFOR we develop, in the fourth section of this paper, several industrial applications.

2. THE COUPLED EULERIAN–LAGRANGIAN FORMULATION

In this section we briefly describe the basis of our simulation procedure:

- The Eulerian formulation that models the rolled plates deformation using the flow formulation implemented via Thompson's pseudo-concentrations technique.
- The coupling of that Eulerian formulation to the Lagrangian formulation that models the rolls deformation (to be developed in the next section).

2.1. The Eulerian formulation

We use a fixed mesh with the material moving inside the mesh; at each point interior to the mesh we define a variable named *pseudo-concentration* (c):

$c \geqslant 0 \Leftrightarrow$ there is material at the point,
$c < 0 \Leftrightarrow$ there is no material at the point.

With ($\dot{\mathbf{u}}$) being the velocity field inside the mesh, the c-distribution fulfils the following equations:

$$\dot{\mathbf{u}} \cdot \nabla c = 0 \quad \text{(stationary problems)} \tag{1a}$$

$$\frac{\partial c}{\partial t} + \dot{\mathbf{u}} \cdot \nabla c = 0 \quad \text{(transient problems)} \tag{1b}$$

For modelling the rolled steel behaviour we use a rigid-viscoplastic constitutive relation [11]; the material flow is described via a viscoplastic-associated von Mises model. Hence, the material flow is incompressible.

We impose the incompressibility constraint via an augmented Lagrangian procedure [12–17]. Equilibrium is reached via an iterative procedure because:

- the material constitutive relation is non-linear;
- the augmented Lagrangian technique iteratively builds the pressure field.

We use a modified Uzawa's algorithm [14] and in the same iterative loop we solve the non-linearities coming from the constitutive model and make the augmentation procedure.

The equations for the kth equilibrium iteration, obtained using the Principle of Virtual Work and the augmented Lagrangian technique are [2]

$$
\int_V 2\mu^{(k-1)} \Delta\dot{\varepsilon}'_{ij} \delta\Delta\dot{\varepsilon}'_{ij} \, dv + \int_V \varkappa\Delta\dot{\varepsilon}_v \delta\Delta\dot{\varepsilon}_v \, dv
$$
$$
= \int_V f_i^v \delta\Delta\dot{u}_i \, dv + \int_{S_\sigma} t_i \delta\Delta\dot{u}_i \, dv
$$
$$
- \int_V s_{ij}^{(k-1)} \delta\Delta\dot{\varepsilon}'_{ij} \, dv - \int_V (p^{(k-1)} + \varkappa\dot{\varepsilon}_v^{(k-1)}) \delta\Delta\dot{\varepsilon}_v \, dv \tag{2}
$$

and

$$
\dot{u}_i^{(k)} = \dot{u}_i^{(k-1)} + \Delta\dot{u}_i^{(k)} \tag{3a}
$$
$$
\dot{\varepsilon}_{ij}^{\prime(k)} = \dot{\varepsilon}_{ij}^{\prime(k-1)} + \Delta\dot{\varepsilon}_{ij}^{\prime(k)} \tag{3b}
$$
$$
\dot{\varepsilon}_v^{(k)} = \dot{\varepsilon}_v^{(k-1)} + \Delta\dot{\varepsilon}_v^{(k)} \tag{3c}
$$
$$
p^{(k)} = p^{(k-1)} + \varkappa\dot{\varepsilon}_v^{(k)} \tag{3d}
$$

In the above equations,

s_{ij} are the deviatoric stress components,

p the hydrostatic stress component,

$\dot{\varepsilon}'_{ij}$ the deviatoric strain rate components (viscoplastic strain rate tensor),

$\dot{\varepsilon}_v$ the volumetric strain rate component (it is constrained to be zero),

$\varkappa$ the penalty parameter; the advantage of the augmented Lagrangian procedure over a standard penalty procedure is the possibility of using smaller values for this parameter and therefore the possibility of working with better conditioned matrices. In Reference [2] we present several numerical examples in which we show the better performance of the augmented Lagrangian procedure as compared with the standard penalty procedure,

μ the viscosity, derived using the constitutive viscoplastic relation [7]. For the special case of a rigid-plastic material we get

$$
\mu = \frac{\sigma_y(\bar{\varepsilon})}{3\dot{\bar{\varepsilon}}} \tag{4}
$$

$\dot{\bar{\varepsilon}}$ the material derivative of the equivalent plastic strain.

$$
\dot{\bar{\varepsilon}} = \left(\frac{2}{3}\dot{\varepsilon}_{ij}\dot{\varepsilon}_{ij}\right)^{1/2} \tag{5}
$$
$$
\dot{\bar{\varepsilon}} = \frac{D\bar{\varepsilon}}{Dt} = \frac{\partial\bar{\varepsilon}}{\partial t} + \dot{\mathbf{u}}\cdot\nabla\bar{\varepsilon} \tag{6}
$$

f_i^v the external forces acting on the body, per unit volume of the spatial configuration,

t_i the external surface forces acting on the body,

V the volume of the body spatial configuration ($c > 0$). However, in order to be able to integrate over the complete mesh, at those points where $c < 0$ we use $\mu = 10^{-3}\mu_{\text{actual material}}$ and

S_σ is the external surface where loads are prescribed.

In Equation (3d) we iteratively build the pressure field using the augmented Lagrangian technique.

For discretizing the equilibrium equations (2) we use finite elements based on the method of *mixed interpolation of tensorial components*. For 2D problems we use the *QMITC-3F* quadrilateral element, which was described in Reference [2] and for 3D problems we use the (*H1-P0*)-*3F* element described in Reference [6]. Both element formulations fulfil the following requirements.

- They satisfy Irons' Patch Test.
- They do not contain spurious zero energy modes.
- They do not lock due to the incompressibility constraint.

For discretizing the transport equations (1a) or (1b) we use standard isoparametric elements: quadrilateral (Q_1) elements for the 2D problems and hexahedral (H_1) elements for the 3D problems. In all cases, for solving the advective transport equations we use the SUPG technique [17, 18].

The equivalent plastic strains are obtained integrating the following equations:

$$\dot{\mathbf{u}} \cdot \boldsymbol{\nabla} \bar{\varepsilon} = \frac{\langle c \rangle}{|c|} \dot{\bar{\varepsilon}} \quad \text{(stationary problems)} \tag{7a}$$

$$\frac{\partial \bar{\varepsilon}}{\partial t} + \dot{\mathbf{u}} \cdot \boldsymbol{\nabla} \bar{\varepsilon} = \frac{\langle c \rangle}{|c|} \dot{\bar{\varepsilon}} \quad \text{(transient problems)} \tag{7b}$$

Some notes regarding our Eulerian formulation are given below.

- The material moves inside a fixed mesh.
- It provides the free surfaces in stationary and transient problems without any special free surface algorithm.
- It does not require a remeshing algorithm, usually needed when using Lagrangian or Eulerian–Lagrangian formulations.

The contact problem between the blank and the tools (plate and work rolls) is modelled using c-dependent boundary conditions [1]; for $\dot{u}_n$, the velocity component normal to a tool surface, we use:

$$c < 0 \Rightarrow \dot{u}_n = \text{free} \tag{8a}$$

$$c \geqslant 0 \Rightarrow \dot{u}_n = 0 \tag{8b}$$

For modelling the friction between the rolls and the steel plates we use either a constant friction law or a Coulomb friction law [19]. It is important to notice that the location of the non-slip points is an analysis result [5].

2.2. Staggered iterative solution

The coupling between the Eulerian model that we described in the previous subsection and the Lagrangian rolls deformation model that we are going to describe in the following section is performed via an iterative staggered scheme that is composed by

- an OUTER LOOP that incorporates the rolls deformation model;
- an INNER LOOP or equilibrium loop.

We describe the staggered iterative scheme in what follows:

OUTER LOOP
1. $k = 0$
2. *Assume for the rolls a trial deformation* $\rightarrow (\mathbf{U}_{\text{rolls}}^{(k)})$
3. $k = k+1$
4. *Keep fixed* $(\mathbf{U}_{\text{rolls}}^{(k-1)})$ *and solve the equilibrium equations (either stationary flow or transient flow, in the latter case solve for the step* $t \rightarrow t+\Delta t$) *GO TO THE INNER LOOP*
5. *From the above loop get the loads imposed by the rolled plates on the rolls* $(\mathbf{R}^{(k)})$
6. *Solve the enhanced beam model under the loads* $\mathbf{R}^{(k)}$ *and the bending forces* $\rightarrow (\mathbf{U}_{\text{rolls}}^{(k)})$

7. *IF* $\dfrac{\|\mathbf{U}_{\text{rolls}}^{(k)} - \mathbf{U}_{\text{rolls}}^{(k-1)}\|_2}{\|\mathbf{U}_{\text{rolls}}^{(k)}\|_2} \leqslant UTOL$

   THEN $\rightarrow CONVERGENCE$
   ELSE $\rightarrow GO\ TO\ 3$

INNER LOOP (EQUILIBRIUM LOOP)
- For stationary problems start from a trial c-distribution and zero velocities $\dot{\mathbf{u}}^{(0)} = 0$.
- For transient problems, $t \rightarrow t + \Delta t$, start from the converged solution at time t.
- Keep constant the rolls deformations (point 4 in the outer loop).

1. $l = 0$
2. $l = l+1$
2.a. $r = 0$; $\dot{\mathbf{u}}^{(r)} = \dot{\mathbf{u}}^{(l-1)}$
2.b. $r = r+1$
   Solve Equations (2) *and* (3a)–(3d) *keeping constant the* c-*distribution and the* $\bar{\varepsilon}$-*distribution.*

2.c. *IF* $\dfrac{\|\dot{\mathbf{u}}^{(r)} - \dot{\mathbf{u}}^{(r-1)}\|_2}{\|\dot{\mathbf{u}}^{(r)}\|_2} \leqslant \dot{U}TOL$ *.AND.* $\|\dot{\bar{\varepsilon}}_v\|_\infty \leqslant \dot{V}TOL$

   THEN $\rightarrow \dot{\mathbf{u}}^{(l)} = \dot{\mathbf{u}}^{(r)}$ *GO TO* 3
   ELSE GO TO 2.b
3. *Calculate the* c-*distribution and the* $\bar{\varepsilon}$-*distribution using Equations* (1a) *or* (1b) *and* (7a) *or* (7b)
4. *IF* $l = 1$
   THEN GO TO 2
   ELSE
      IF $\dfrac{\|\dot{\mathbf{u}}^{(l)} - \dot{\mathbf{u}}^{(l-1)}\|_2}{\|\dot{\mathbf{u}}^{(l)}\|_2} \leqslant \dot{U}TOL$
   THEN $\rightarrow CONVERGENCE$
   ELSE $\rightarrow GO\ TO$ 2

3. SIMULATION OF THE ROLLS DEFORMATION. THE ENHANCED BEAM MODEL

In this section we present the enhanced beam model that we developed to simulate the rolls elastic deformation.

3.1. Contact between work and back-up rolls. The Hertz elements

We discretize the work roll and its corresponding back-up roll using Hermitian beam elements that include the shear deformation [20]. In the area where contact between both rolls is possible we define pairs of matching nodes (one on each beam model) and between them we implement a 'node-to-node' contact algorithm (usually the rolls are parallel and the matching nodes are located at the intersections between the beam axes and a common normal). We interpose between the matching nodes an ad hoc element that models the flattening of both surfaces in contact: our new *Hertz element*.

For the ith Hertz element connecting the matching nodes N_i^w (corresponding to the work roll) and N_i^b (corresponding to the back-up roll), using the nomenclature in Figure 3, we define the initial gap,

$$\delta_i^0 = |\mathbf{r}_{N_i^w} - \mathbf{r}_{N_i^b}| - (R_i^w + R_i^b) \tag{9}$$

please notice that due to the rolls mechanical and thermal crown the radii (R_i^w and R_i^b) are variable from node to node.

Loading the beam system (work+back-up rolls) with the forces determined in the Eulerian model plus the bending forces, we get the nodal displacements $\mathbf{U}_{N_i^w}$ and $\mathbf{U}_{N_i^b}$; hence, the gap undergoes a change, from δ_i^0 to $(\delta_i^0 + \Delta_U \delta_i)$,

$$\Delta_U \delta_i = (\mathbf{U}_{N_i^b} - \mathbf{U}_{N_i^w}) \cdot \mathbf{r}_i = u_i^b - u_i^w \tag{10}$$
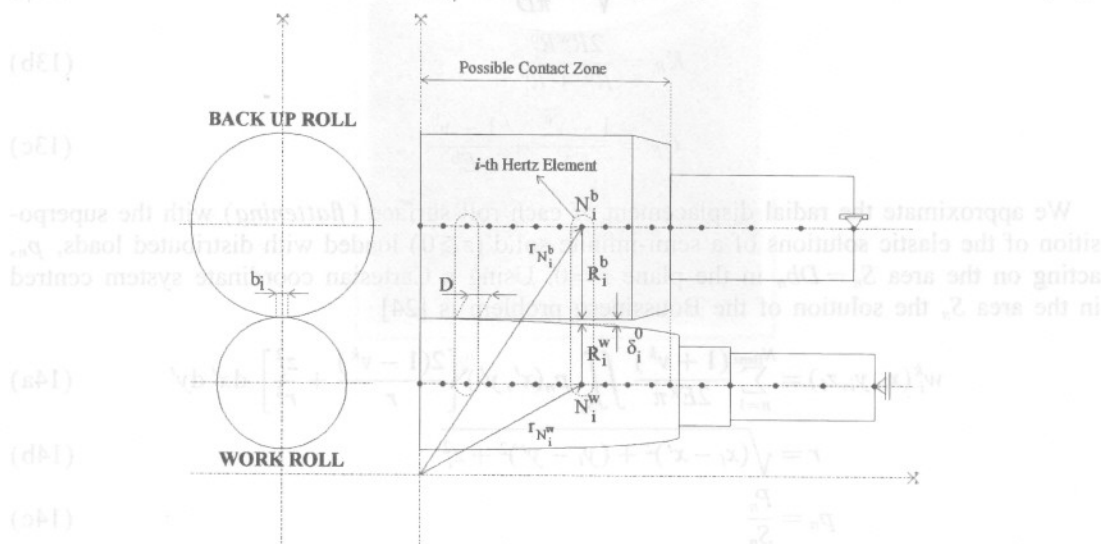

Figure 3. Definition of a Hertz element.

where

$$\mathbf{r}_i = \frac{\mathbf{r}_{N_i^b} - \mathbf{r}_{N_i^w}}{|\mathbf{r}_{N_i^b} - \mathbf{r}_{N_i^w}|}$$

The gap is also affected by the Poisson effect in the bent beams [21],

$$\Delta_v \delta_i = (\mathbf{U}_{N_i^b}^v - \mathbf{U}_{N_i^w}^v) \cdot \mathbf{r}_i = u_i^{v^b} - u_i^{v^w} \tag{11a}$$

$$\left| \mathbf{U}_{N_i^k}^v \right| = \frac{v^k |\mathbf{M}_i^k| (R_i^k)^2}{2 E^k I_i^k} \tag{11b}$$

the second equation was obtained from Reference [22] and both displacements act in the direction of the bending displacements but with opposite sense. In the above equation,

E^k, v^k　are the Young's modulus and Poisson ratio for the work roll ($k = w$) or for the back-up roll ($k = b$) and

$\mathbf{M}_i^k, I_i^k$　the bending moment and inertia moment for the work roll/back-up roll section related to the ith Hertz element.

Therefore, the rolls bending makes the initial gap evolve from δ_i^0 to the value

$$\delta_i^1 = \delta_i^0 + \Delta_U \delta_i + \Delta_v \delta_i \tag{12}$$

When $\delta_i^1 > 0$ the nodes N_i^w and N_i^b are not in contact and when $\delta_i^1 < 0$ both nodes are in contact and there is a contact force (P_i) among them. With D being the axial distance between equally spaced nodes on the roll axes and b_i the width of the contact zone for the $N_i^w - N_i^b$ Hertz element, we can write [23]

$$b_i = \sqrt{\frac{2 P_i K_{R_i} C_E}{\pi D}} \tag{13a}$$

$$K_{R_i} = \frac{2 R_i^w R_i^b}{R_i^w + R_i^b} \tag{13b}$$

$$C_E = \frac{1 - v^w}{E^w} + \frac{1 - v^b}{E^b} \tag{13c}$$

We approximate the radial displacement of each roll surface (*flattening*) with the superposition of the elastic solutions of a semi-infinite solid ($z \geqslant 0$) loaded with distributed loads, p_n, acting on the area $S_n = D b_n$ in the plane $z = 0$. Using a Cartesian coordinate system centred in the area S_n the solution of the Boussinesq problem is [24]

$$w_i^k(x_i, y_i, z_i) = \sum_{n=1}^{N_{\text{Hertz}}} \frac{(1 + v^k)}{2 E^k \pi} \iint_{S_n} p_n(x', y') \left[\frac{2(1 - v^k)}{r} + \frac{z_i^2}{r^3} \right] \mathrm{d}x' \, \mathrm{d}y' \tag{14a}$$

$$r = \sqrt{(x_i - x')^2 + (y_i - y')^2 + z_i^2} \tag{14b}$$

$$p_n = \frac{P_n}{S_n} \tag{14c}$$

where N_{Hertz} is the number of Hertz elements.

With a close-form solution we can calculate the integral on the r.h.s. of Equation (14a). The contribution of each roll ($k = $ w or b) to the flattening of the ith Hertz element is

$$a_i^k = w_i^k(0,0,0) - w_i^k(0,0,R) \qquad (15)$$

The flattening of the ith Hertz element is the addition of all the contributions we evaluated above; hence, the gap evolves from its original value to a final value,

$$\delta_i = \delta_i^0 + \Delta_U\delta_i + \Delta_v\delta_i + a_{i1} + a_{i2} = \delta_i^1 + a_{i1} + a_{i2} \qquad (16a)$$

the contact condition imposes

$$\delta_i = 0 \qquad (16b)$$

For solving the non-linear beam system we implemented the following algorithm:

1. $m = 0$
2. *Load the work roll with the forces calculated in the rigid-viscoplastic model, with the bending forces and with a back-up roll reaction assumed uniform for the first trial ($P_i^{(0)}$, $i = 1, N_{\text{Hertz}}$ are the equivalent contact forces)*
3. *Load the back-up roll with the assumed uniform reaction ($P_i^{(0)}$, $i = 1, N_{\text{Hertz}}$)*
4. *Calculate the gap of the Hertz elements ($i = 1, N_{\text{Hertz}}$) using in Equation (16a) the nodal loads $\mathbf{P}^{(m)}$*
5. *IF for all the Hertz elements $\delta_i^1 \geqslant 0$ ($i = 1, N_{\text{Hertz}}$) THEN GO TO 7*
6. *Correct the contact force distribution at the M nodes where $\delta_i < 0$ imposing Equation (16b)*

6.a.
$$\mathbf{K}\Delta\mathbf{P}^{(m)} = -\boldsymbol{\delta} \quad (M \times M \ system)$$

where
$$\boldsymbol{\delta}^{\mathrm{T}} = [\delta_1 \quad \delta_2 \quad \cdots \delta_M]$$

$$K_{pq} = \frac{\partial\delta_p}{\partial P_q} = \frac{\partial\Delta_U\delta_p}{\partial P_q} + \frac{\partial\Delta_v\delta_p}{\partial P_q} + \frac{\partial a_{p1}}{\partial P_q} + \frac{\partial a_{p2}}{\partial P_q}$$

6.b. $m = m + 1$
6.c. $\mathbf{P}^{(m)} = \mathbf{P}^{(m-1)} + \Delta\mathbf{P}^{(m)}$
6.d. *IF $P_i^{(m)} < 0$ THEN $P_i^{(m)} = 0$, $i = 1, M$*

6.e. *IF* $\dfrac{\|\mathbf{P}^{(m)} - \mathbf{P}^{(m-1)}\|_2}{\|\mathbf{P}^{(m)}\|_2} \leqslant PTOL \ THEN \ GO \ TO \ 7$

ELSE GO TO 4

7. *CONVERGENCE*

3.2. Contact between work rolls and the rolled plates

In order to determine the total rolls deformation it is necessary to add, to the deformation calculated as detailed above, the flattening of the work rolls due to their contact with the rolled steel plates. For this purpose we use Equation (14a) integrated over the contact surface between the work roll and the rolled steel plate.

4. INDUSTRIAL APPLICATIONS OF THE MODEL

In this section we present several simulations developed, for the hot rolling mill in Figure 1, using our modelling procedure. Our objectives are to qualify, for roughing and finishing stands, the developed finite element technique and to demonstrate its potential for predicting, in actual engineering applications, the plate profiles that can be expected when using different set-up alternatives in the rolling mill. The analyses that we describe in what follows need to render very accurate results because, in the modern industrial practice, the boundary between acceptable plate profiles and non-acceptable ones is defined by profile differences from two to three orders of magnitude smaller than the plates thickness.

As it is well known, the solution of the transport equation (1a) or (1b), that defines the plates profile, usually does not provide the needed accuracy due to numerical diffusions that can be minimized, using the available numerical techniques [17, 18], but not completely eliminated, specially in the case of non-regular meshes. However, in our numerical experimentation we found that this lack of accuracy in determining the position of the surfaces $c = 0$, that define the plates geometry, does not have an important influence when calculating the separating forces; hence, the most accurate procedure for determining the rolled plates profile is by considering the model predictions for the work rolls deformation.

4.1. Validation of the model for a roughing stand (R4)

In References [3, 4, 6] we published the result of a set of industrial tests that were developed for validating our finite element model when applied to a roughing stand. The industrial tests were carried out on the roughing stand R4 and the obtained results are reproduced in Figure 4. The larger difference between the finite element predicted plate profile at the stand exit and the measured plate profile at that point is located at approximately ± 450 mm from the stand
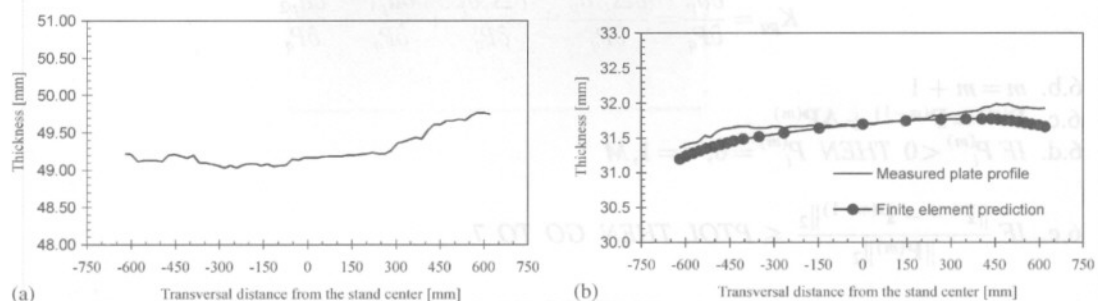

Figure 4. Validation of the model for a roughing stand: (a) upstream measured plate profile; (b) downstream measured plate profile and finite element prediction.
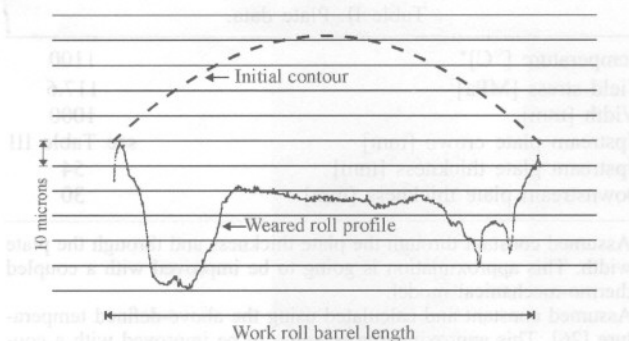
Figure 5. R4 roll wear profile.

Table I. Rolls data.

	Back-up rolls	Work rolls
Material	Steel	Casted iron
E [GPa]	205.8	172.5
Central diameter [mm]	1185.86	622.94
Total crown [mm]	0.00	see Table III
Peripheral speed [m/s]		2.136

centre. This is because in our analysis, we did not incorporate into the model geometry the rolls wear, which can be characterized with the typical R4 roll wear profile shown in Figure 5.

The obtained results are quite satisfactory and therefore we can consider that METFOR is a valid tool for modelling a roughing stand.

4.2. Parametric analyses on a roughing stand (R4)

The purpose of these analyses is to investigate the effects, on the plate profile produced at this roughing stand, of:

- The plate profile at the stand entrance (that is to say the plate profile produced by the upstream stand R3)
- The total crown of the work rolls.[§]

For our analyses we considered the stand data given in Tables I and II.
In our parametric analysis we considered the cases given in Table III.
In all cases we considered a constant friction law with $m = 0.7$.
In Figure 6 we present for the six analysed cases the 'plate–work rolls' separating force distribution.

[§] The concept of roll crown will be discussed in Appendix A.

Table II. Plate data.

Temperature [°C]*	1100
Yield stress [MPa]†	117.6
Width [mm]	1000
Upstream plate crown [mm]	see Table III
Upstream plate thickness [mm]	54
Downstream plate thickness [mm]	30

* Assumed constant through the plate thickness and through the plate
  width. This approximation is going to be improved with a coupled
  thermo-mechanical model.
† Assumed constant and calculated using the above-defined tempera-
  ture [26]. This approximation is going to be improved with a cou-
  pled thermo-mechanical–metallurgical model.

Table III. Parametric analysis.

Case	Total crown of the work rolls [mm]	Upstream plate crown [mm]
1	+0.1	0.0
2	+0.1	+0.4
3	+0.1	−0.4
4	−0.1	0.0
5	−0.1	+0.4
6	−0.1	−0.4
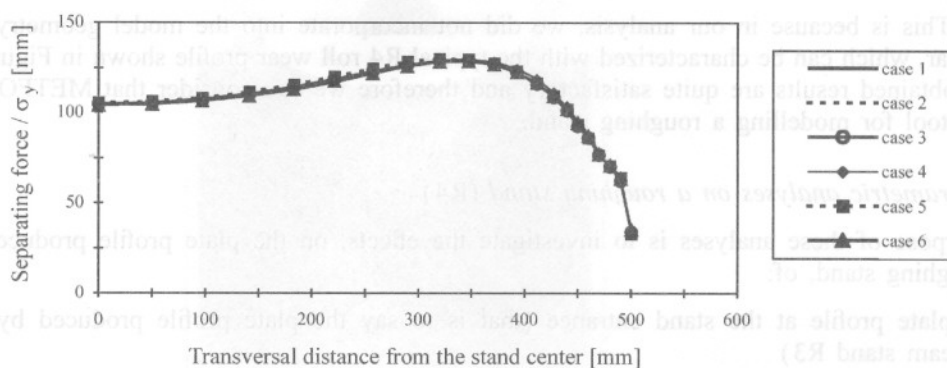
Figure 6. R4 parametric analysis.

From the results plotted above we conclude the following:

- The separating force distribution is not dependent on the plate profile upstream of the
  stand R4.
- Since the roll deformation (bending and flattening) is determined by the separating forces,
  and the plate profile downstream of the stand R4 is determined by the roll deformation, we

can conclude that for this stand the produced plate profile is not dependent on the incoming plate profile.

4.3. Validation of the model for a finishing stand (F10)

In this subsection we present the qualification of our finite element model for the analysis of a finishing stand, comparing its predictions with actual industrial measurements performed on the rolling mill.

It is very important to include in the analysis an accurate description of the rolls thermal crown;[¶] hence, to analyse the rolls thermal evolution and the corresponding thermal crown evolution we developed the finite element system TCROWN, described elsewhere [25], composed of two modules:

- ROLLTEM: predicts the work rolls thermal evolution. It is a 2D axisymmetric finite element model. Even though the axisymmetric model cannot predict the temperature peaks on the roll surface, these peaks have a very low thickness penetration [10] and can be neglected for determining the rolls thermal expansion.
- ROLLEXP: calculates, using a thermo-elastic model, the work rolls thermal crown evolution.

Using TCROWN, and measurements of the rolls surface temperature performed after the rolling schedule described in Figure 7, we characterized the work rolls thermal evolution as shown in the same figure.

In Plate 1 we describe the temperature distribution corresponding to the instant at which the last rolled coil exits the F10 stand. In Figure 8 we plot the roll profile developed by the temperature distribution described in the previous figure and the initial cold roll profile, from which the thermal radial expansion and the resulting thermal crown can be obtained.

To perform our finite element analysis we used the following data.

1. Upstream plate profile with a relative crown (*crown/thickness*)[||] equal to the relative crown measured on the downstream plate profile.
2. Plate constant yield stress (200.9 MPa) calculated matching the measured total separating force (8124.2 kN) with the numerically predicted total separating force.
3. Bending force $F_1 = 156.8$ kN; $F_2 = 0$ (see Figure 2).

In Figure 9 we compare the numerical plate profile predicted by METFOR, using the above data, with the distribution of on-line measurements performed on the same plate by the thickness-measuring equipment of the rolling mill.

If instead of calculating the yield stress as described above, we use the expressions in Reference [26] with a stand temperature of 920°C we obtain a total separating force 25% higher than the actual one; even though this discrepancy is of the order of the discrepancies reported in References [27–29] for models that do not include the thermo-mechanical–metallurgical coupling, it is too high for the purpose of predicting the plate profile. Of course,

---

[¶]The concepts of thermal and mechanical rolls crown will be discussed in Appendix A.
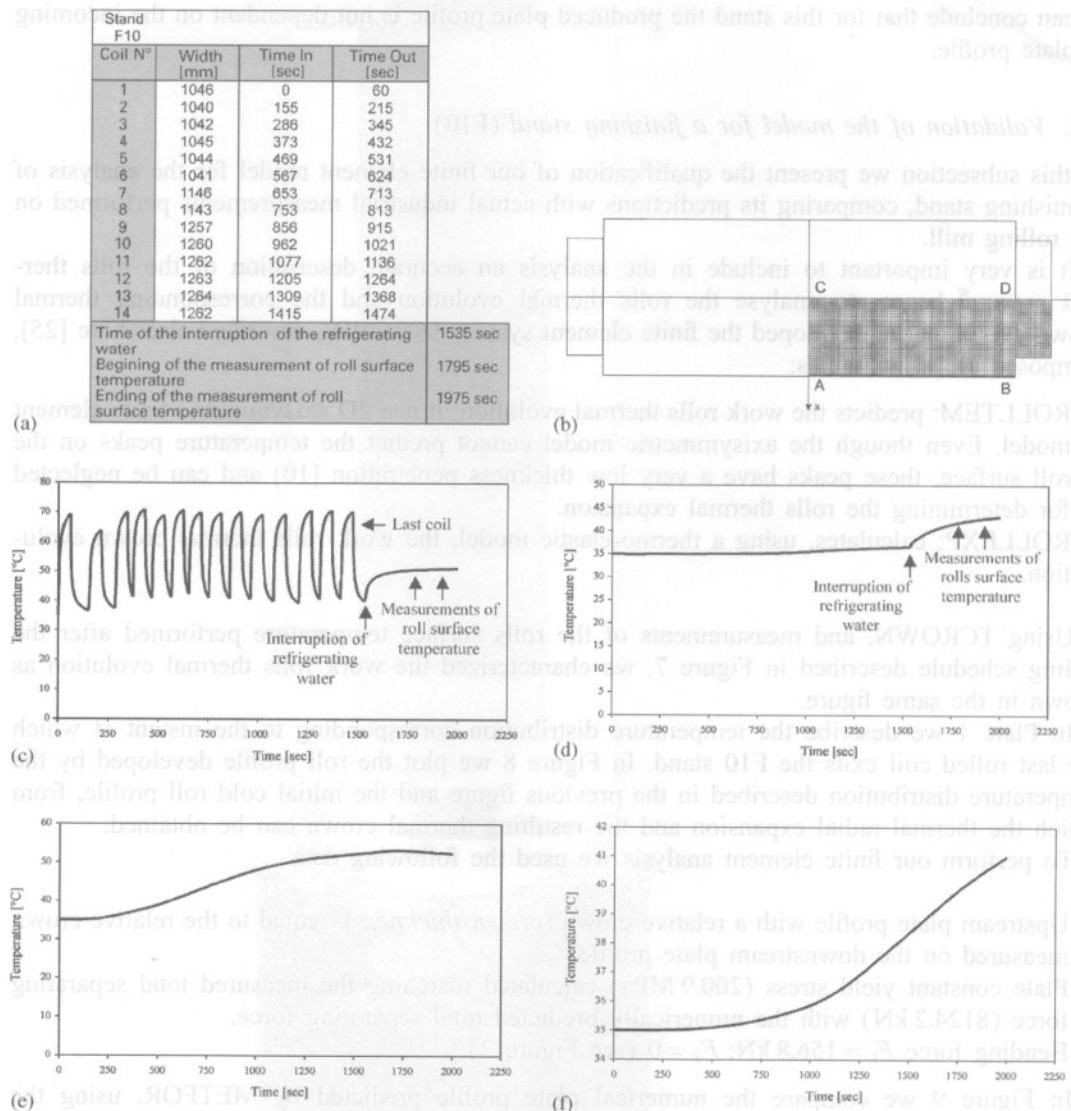[||]The influence of the relative crown on the plate flatness will be discussed in Appendix A.

Stand F10			
Coil N°	Width [mm]	Time In [sec]	Time Out [sec]
1	1046	0	60
2	1040	155	215
3	1042	286	345
4	1045	373	432
5	1044	469	531
6	1041	567	624
7	1146	653	713
8	1143	753	813
9	1257	856	915
10	1260	962	1021
11	1262	1077	1136
12	1263	1205	1264
13	1264	1309	1368
14	1262	1415	1474
Time of the interruption of the refrigerating water			1535 sec
Begining of the measurement of roll surface temperature			1795 sec
Ending of the measurement of roll surface temperature			1975 sec

(a)

(b)

(c)

(d)

(e)

(f)

Figure 7. Simulation of the work rolls thermal evolution: (a) rolling schedule; (b) work roll finite element model (axisymmetric model); (c) thermal evolution at point A (numerical simulation result); (d) thermal evolution at point B (numerical simulation result); (e) thermal evolution at point C (numerical simulation result); (f) thermal evolution at point D (numerical simulation result).

when we implement a coupled thermo-mechanical–metallurgical model we will not need to go through the measurement and matching of the separating forces.

The obtained results are quite satisfactory and therefore we can consider that METFOR is also a valid tool for modelling a finishing stand.

Temperature [°C]

(a)

(b)

(c)
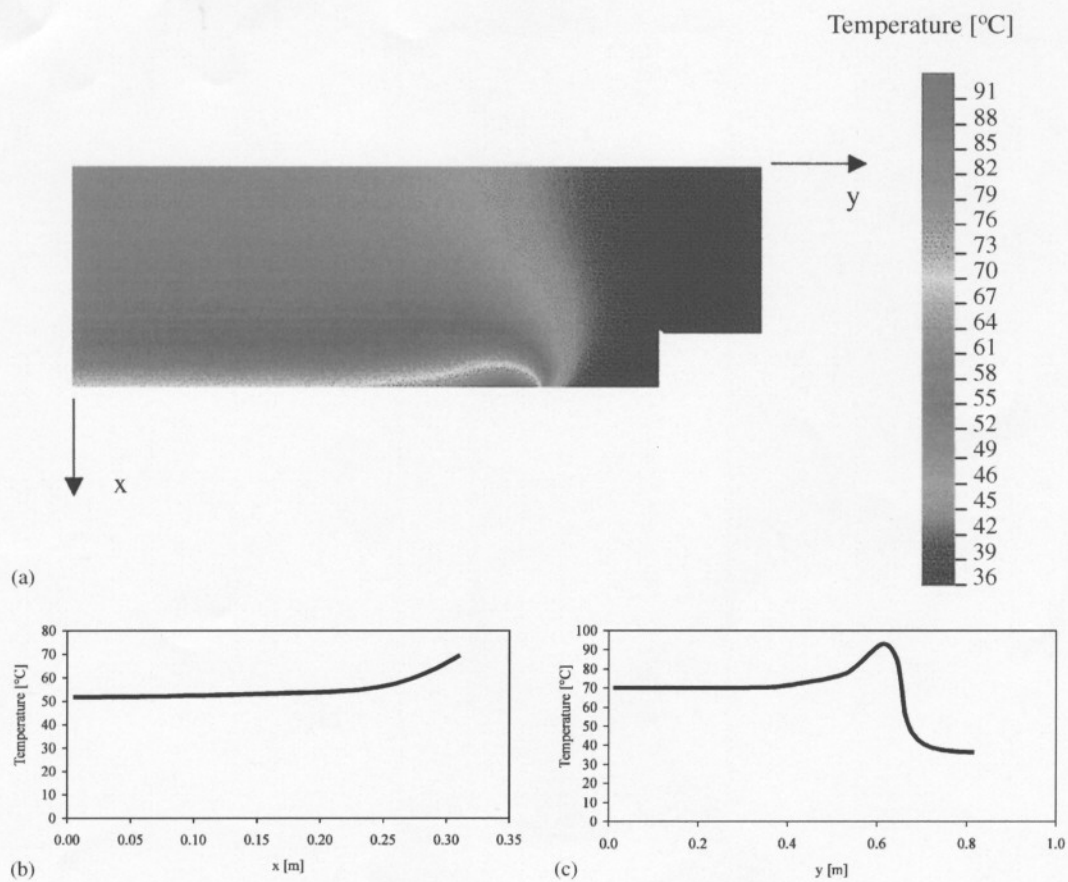
Plate 1. Work rolls temperature distribution: (a) temperature map of the work roll at the instant at which the last coil exits the stand F10 (t_{out}); (b) work roll radial temperature distribution ($y = 0$) at t_{out}; (c) work roll surface temperature distribution at t_{out}.
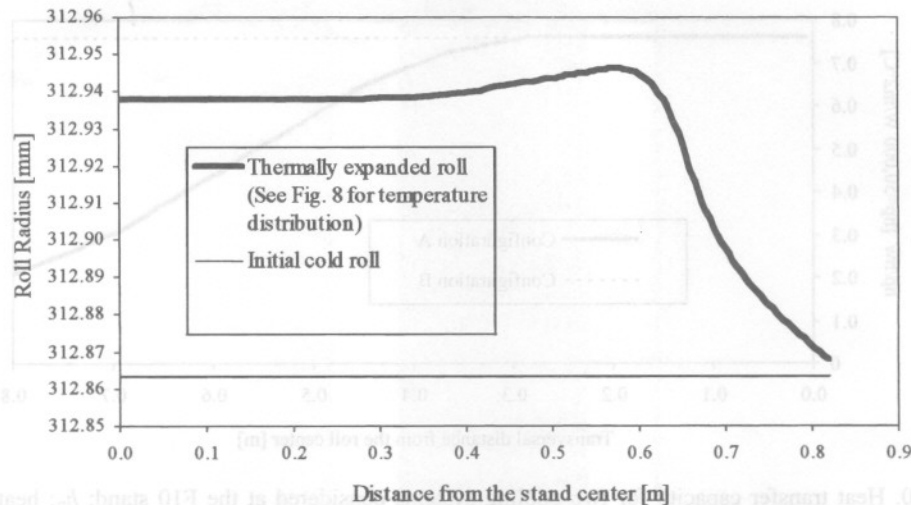
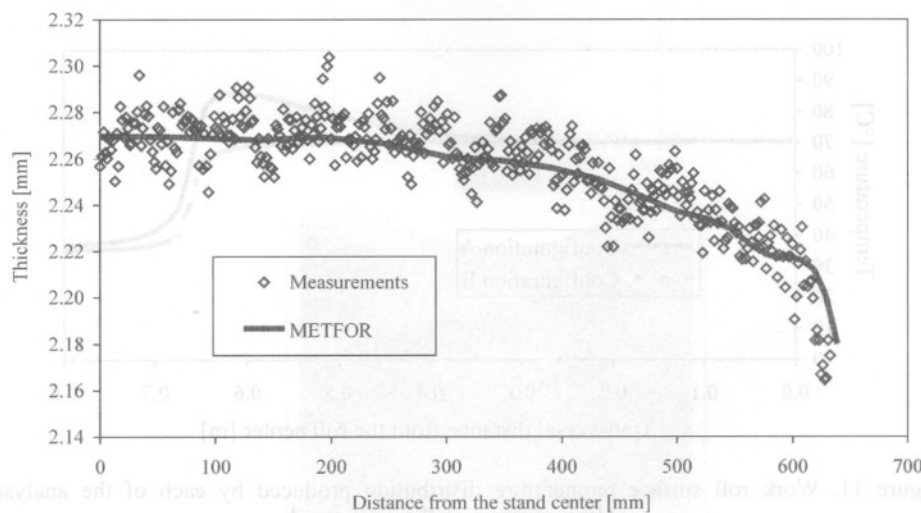Figure 8. Work roll profile at the F10 stand predicted using TCROWN.

Figure 9. Validation of the finite element results for the F10 stand.

4.4. *Parametric analyses on a finishing stand* (F10)

In this subsection we analyse the plate profile produced in the last finishing stand when two different strategies are used for cooling the work rolls; in Figure 10 we represent, for each of the two water cooling configurations that we are going to consider, its heat transfer capacity distribution.
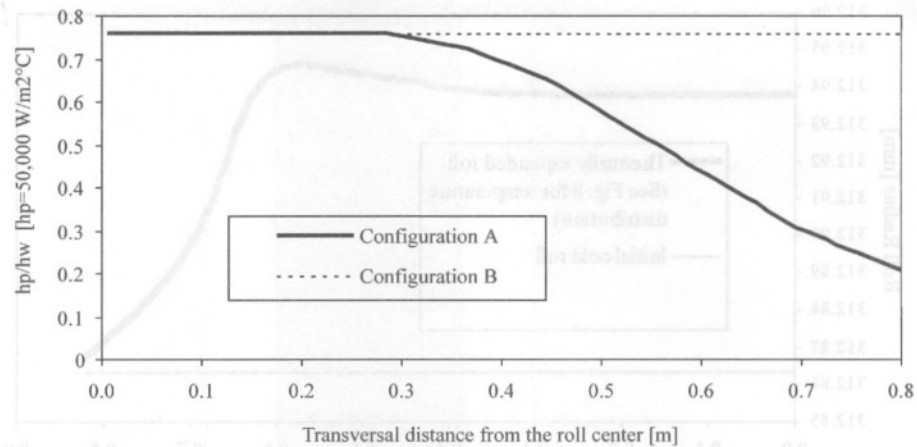
Figure 10. Heat transfer capacity for two cooling systems considered at the F10 stand: h_p: heat transfer coefficient between plate and roll (assumed constant); h_w: cooling water heat transfer coefficient.
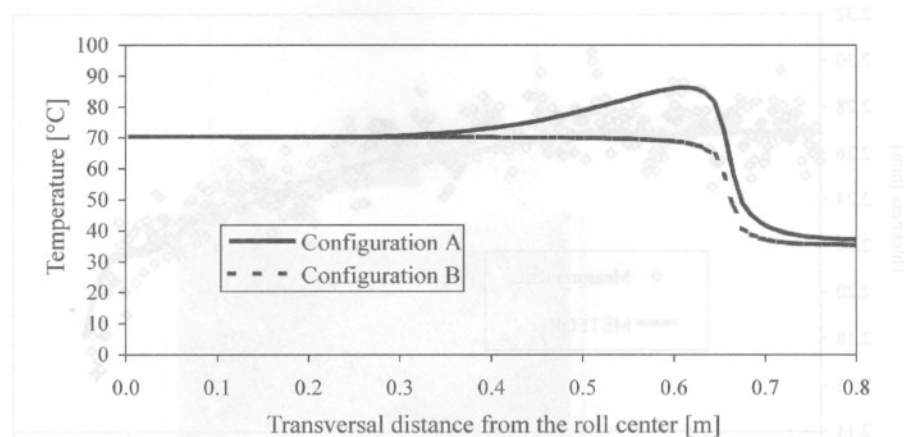
Figure 11. Work roll surface temperature distribution produced by each of the analysed cooling systems at the F10 stand.

Using the finite element system TCROWN we evaluate the work roll temperature distributions (Figure 11) and the work roll profiles (Figure 12) after rolling 14 plates. Using the data in Figure 12 we analyse the stand with METFOR and obtain the results in Figure 13. It is evident that, in the case of a finishing stand, the rolls cooling system has a strong control on the produced plate profiles and therefore on the plate flatness [10].
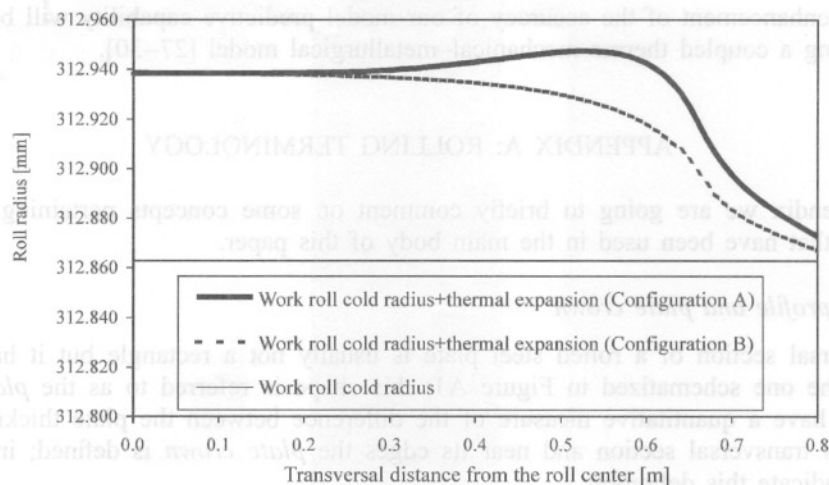
Figure 12. Work roll profiles produced by each of the analysed cooling systems at the F10 stand.
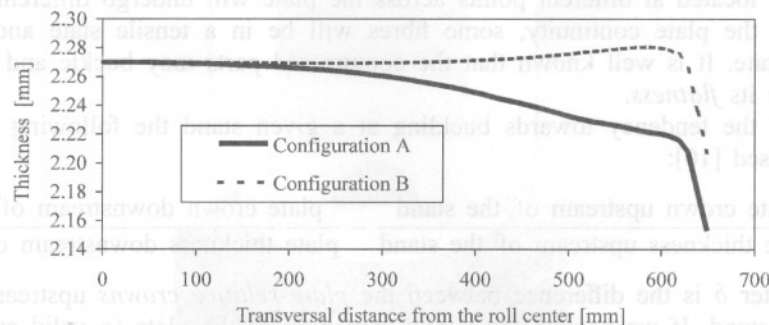
Figure 13. Plate profiles predicted by METFOR for each of the two cooling systems considered.

5. CONCLUSIONS

We presented a finite element formulation for modelling the hot rolling of steel plates; the formulation couples an Eulerian description of the rolled plates deformation and a Lagrangian description of the rolls deformation.

The Eulerian description of the rolled plates deformation is developed using the classical flow formulation (rigid-viscoplastic material model) implemented via Thompson's pseudo-concentrations technique.

The Lagrangian description of the rolls deformation is developed using a new enhanced beam element; the Hertz element incorporates the bending deformation of the work rolls supported by the back-up rolls and the flattening of the contact areas. It is a non-linear elastic element and it is much more efficient than the 3D elements.

A future enhancement of the accuracy of our model predictive capability will be achieved by developing a coupled thermo-mechanical–metallurgical model [27–30].

APPENDIX A: ROLLING TERMINOLOGY

In this appendix we are going to briefly comment on some concepts pertaining to rolling technology that have been used in the main body of this paper.

A.1. Plate profile and plate crown

The transversal section of a rolled steel plate is usually not a rectangle but it has a shape similar to the one schematized in Figure A1; this shape is referred to as the *plate profile*. In order to have a quantitative measure of the difference between the plate thickness at the centre of its transversal section and near its edges the *plate crown* is defined; in the same figure we indicate this definition.

A.2. Plate flatness

Since the transversal section of a plate is of variable thickness, it is apparent that during rolling different fibres located at different points across the plate will undergo different elongations; hence, due to the plate continuity, some fibres will be in a tensile state and others in a compressive state. It is well known that the compressed parts may buckle and therefore the plate may lose its *flatness*.

To quantify the tendency towards buckling at a given stand the following technological parameter is used [10]:

$$\delta = \frac{\text{plate crown upstream of the stand}}{\text{plate thickness upstream of the stand}} - \frac{\text{plate crown downstream of the stand}}{\text{plate thickness downstream of the stand}}$$

The parameter δ is the difference between the *plate relative crowns* upstream and downstream of the stand. If we neglect the lateral spreading of the plate (a valid assumption for the last finishing stands) then,

- $\delta < 0$ indicates a tendency towards buckling at the plate edges,
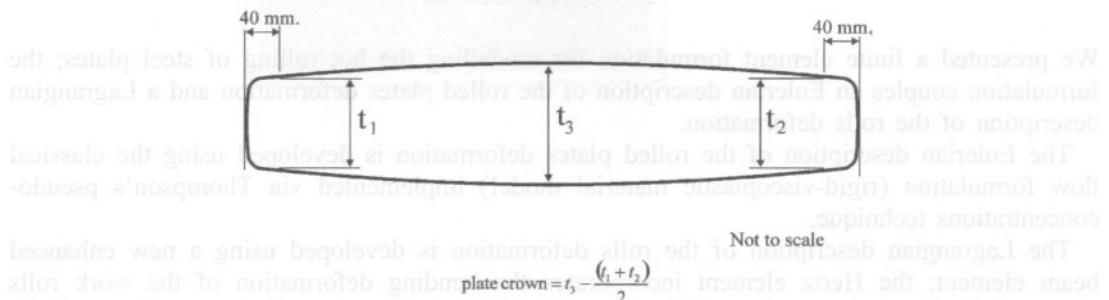- $\delta > 0$ indicates a tendency towards buckling at the plate centre.

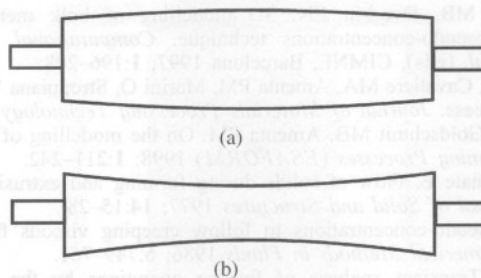Figure A1. Plate profile and crown: plate crown $= t_3 - \frac{(t_1 + t_2)}{2}$.

Figure A2. Rolls profile and crown: (a) roll with positive crown; (b) roll with negative crown; roll crown = centre diameter − edge diameter.

Therefore, the objective of a stand set-up is a rolling condition with $\delta = 0$ in order to produce a flat plate. However, a range inside which the flatness of the plate can be assured has been experimentally defined [10]:

$$-80 \left[\frac{\text{downstream thickness}}{\text{plate width}} \right]^{1.86} < \delta < 40 \left[\frac{\text{downstream thickness}}{\text{plate width}} \right]^{1.86}$$

A.3. Rolls profile and crown

The work rolls and sometimes also the back-up rolls are not straight cylinders; usually, the cylinder generatrices have a shape similar to the ones indicated in Figure A2 (*roll profiles*), to compensate the bending of the rolls and therefore produce a plate with a smaller crown. The number used to define a roll profile is the *roll crown* whose definition is also indicated in the same figure.

As already discussed in the fourth section, the thermal evolution of the work rolls during rolling imposes an evolution of their shape, and hence the original or *mechanical crown* of the rolls is modified by a *thermal crown*; therefore,

$$total \; crown = mechanical \; crown + thermal \; crown$$

ACKNOWLEDGEMENTS

REFERENCES

1. Dvorkin EN, Petöcz EG. An effective technique for modelling 2D metal forming processes using an Eulerian formulation. *Engineering Computations* 1993; **10**:323–336.
2. Dvorkin EN, Cavaliere MA, Goldschmit MB. A three field element via augmented Lagrangian for modelling bulk metal forming processes. *Computational Mechanics* 1995; **17**:2–9.
3. Dvorkin EN, Goldschmit MB, Cavaliere MA, Amenta PM. On the modelling of bulk metal forming processes. *Proceedings of Second ECCOMAS (European Community on Computational Methods in Applied Sciences) Conference on Numerical Methods in Engineering*. John Wiley & Sons: New York, 1996.

4. Cavaliere MA, Goldschmit MB, Dvorkin EN. 3D modelling of bulk metal forming processes via the flow formulation and the pseudo-concentrations technique. *Computational Plasticity—Fundamentals and Applications*, Owen DRJ et al. (eds), CIMNE, Barcelona 1997; **1**:196–208.
5. Dvorkin EN, Goldschmit MB, Cavaliere MA, Amenta PM, Marini O, Stroppiana W. 2D finite element parametric studies of the flat rolling process. *Journal of Materials Processing Technology* 1997; **68**:99–107.
6. Dvorkin EN, Cavaliere MA, Goldschmit MB, Amenta PM. On the modelling of steel product rolling processes. *International Journal of Forming Processes* (*ESAFORM*) 1998; **1**:211–242.
7. Zienkiewicz OC, Jain PC, Oñate E. Flow of solids during forming and extrusion: some aspects of numerical solutions. *International Journal of Solid and Structures* 1977; **14**:15–28.
8. Thompson E. Use of the pseudo-concentrations to follow creeping viscous flows during transient analysis. *International Journal for Numerical Methods in Fluids* 1986; **6**:749–761.
9. Thompson E, Smelser RE. Transient analysis of forging operations by the pseudo-concentrations method. *International Journal for Numerical Methods in Engineering* 1988; **25**:177–189.
10. Ginzburg V. *High-Quality Steel Rolling: Theory and Practice*. Marcel Decker Inc.: New York, 1993.
11. Perzyna P. Fundamental problems in viscoplasticity. *Advances in Applied Mechanics*, Vol. 9. Academic Press: New York, 1996.
12. Felippa CA. Iterative procedures for improving penalty function solutions of algebraic systems. *International Journal for Numerical Methods in Engineering* 1978; **12**:821–836.
13. Zienkiewicz OC, Vilotte JP, Toyoshima S, Nakazawa S. Iterative method for constrained and mixed approximation. An inexpensive improvement of FEM performance. *Computer Methods in Applied Mechanics and Engineering* 1985; **51**:3–29.
14. Fortin M, Fortin A. A generalization of Uzawa's algorithm for the solution of the Navier–Stokes equations. *Communications in Numerical Methods in Engineering* 1985; **1**:205–208.
15. Simo JC, Laursen T. An augmented Lagrangian treatment of contact problems involving friction. *Computers and Structures* 1992; **42**:97–116.
16. Luenberger DG. *Linear and Nonlinear Programming*. Addison-Weley: Reading, MA, 1984.
17. Zienkiewicz OC, Taylor RL. *The Finite Element Method* (4th edn). McGraw-Hill: New York, 1989.
18. Hughes TJR. *The Finite Element Method*. Prentice-Hall: Englewood Cliffs, NJ, 1987.
19. Backofen W. *Deformation Processing*. Addison-Wesley: Reading, MA, 1972.
20. Bathe KJ. *Finite Element Procedures*. Prentice-Hall: Englewood Cliffs, NJ, 1996.
21. Hacquin A, Montmitonnet P, Guillerault JP. Experimental validation of a rolling stand elastic deformation model. *Journal of Materials Processing Technology* 1994; **45**:199–206.
22. Wang CT. *Applied Elasticity*. McGraw-Hill: New York, 1953.
23. Roark RJ, Young WC. *Formulas for Stress and Strain* (5th edn). McGraw-Hill: New York, 1975.
24. Love AEH. *A Treatise on the Mathematical Theory of Elasticity*. Dover Publications: New York, 1944.
25. Dvorkin EN, Cavaliere MA, Zielonka MG, Goldschmit MB. New developments for the modelling of metal rolling processes. *Proceedings of the European Conference on Computational Mechanics, ECCM*, Munich, 1999.
26. Pietrzyk M, Lenard J. *Thermal-Mechanical Modelling of the Flat Rolling Process*. Springer-Verlag: Berlin, 1991.
27. Devadas C, Samarasekera IV, Hawbolt EB. The thermal and metallurgical state of steel strip during hot rolling: Part I. Characterization of heat transfer. *Metallurgical Transactions* 1991; **22A**:307–319.
28. Devadas C, Baragar D, Ruddle G, Samarasekera IV, Hawbolt EB. The thermal and metallurgical state of steel strip during hot rolling: Part II. Factors influencing rolling loads. *Metallurgical Transactions* 1991; **22A**:321–333.
29. Devadas C, Samarasekera IV, Hawbolt EB. The thermal and metallurgical state of steel strip during hot rolling: Part III. Microstructural evolution. *Metallurgical Transactions* 1991; **22A**:335–349.
30. Cavaliere MA, Goldschmit MB, Dvorkin EN. On the solution of thermo-mechanical problems via the pseudo-concentrations technique. *Proceedings of the European Congress on Computational Methods in Applied Sciences and Engineering, ECCOMAS*, Barcelona, 2000.